

## Electronic Supplementary Information

# Effects of solvation shell relaxation on chain association mechanisms in poly(3-hexylthiophene) solutions

Ching H. Wu,<sup>a</sup> Chi C. Hua\*<sup>a</sup> and Chun I Wang<sup>b</sup>

<sup>a</sup>*Department of Chemical Engineering, National Chung Cheng University, Chia-Yi 62102, Taiwan*

<sup>b</sup>*Institute of Chemistry, Academia Sinica, Taipei 115, Taiwan*

### S1 Description and validation of force fields

#### Solvent molecules

For the solvent molecules investigated herein, i.e., *ortho*-dichlorobenzene, bromobenzene, chlorobenzene, chloroform, *para*-xylene and toluene, we followed prior work by Wang *et al.*<sup>1</sup> who utilized OPLS force field<sup>2</sup> and united-atom model (except for chloroform, for which an all-atom description is necessary) in AMD simulations, with partial atomic charges obtained from CDP force field<sup>3,4</sup> for chloroform and TraPPE force field<sup>5,6</sup> for the others; see chemical structures and charge distributions in Fig. S1. According to TraPPE, partial atomic charges of *para*-xylene and toluene were not considered. The properties of *ortho*-dichlorobenzene, bromobenzene, chlorobenzene and chloroform

with (w/) and without (w/o) including partial atomic charges were compared. The results gathered in Table S1 indicated little difference in the computed values of system density ( $\rho$ ), self-diffusion coefficient ( $D$ ) and viscosity ( $\eta$ ), with generally excellent agreement with experimental data available.

For the calculations of solvent viscosity, we first equilibrated 500 solvent molecules for 1 ns in an  $NPT$  ensemble at 300 K and 1 bar to ensure the system density was properly converged. A 20 ns simulation was then carried out in  $NVT$  ensemble at 300 K for data collection. Following the Green-Kubo relation, the solvent viscosity can be evaluated from the time integration of the pressure tensor autocorrelation function:

$$\eta = \frac{V}{k_B T} \int_0^\infty P_{ACF}(t) dt$$

where  $V$  is the volume of the simulation system,  $k_B$  is the Boltzmann constant, and  $T$  is absolute temperature. The autocorrelation function  $P_{ACF}(t)$  bears the form

$$P_{ACF}(t) = \frac{1}{5} \sum_i \langle P_i(t) P_i(0) \rangle$$

where  $P_i$  represents each of the five independent components of the pressure tensor,  $(P_{xx} - P_{yy})/2$ ,  $(P_{yy} - P_{zz})/2$ ,  $P_{xy}$ ,  $P_{yz}$ , and  $P_{zx}$ .<sup>7,8</sup> The element  $\alpha\beta$  of the pressure tensor can be evaluated via

$$P_{\alpha\beta} = \frac{1}{V} \left( \sum_i \frac{P_{i\alpha} P_{i\beta}}{m_i} + \sum_i r_{i\alpha} f_{i\beta} \right)$$

where  $P_{i\alpha}$  is the momentum of particle  $i$  in the direction of  $\alpha$ ,  $m_i$  is its mass,  $f_{i\beta}$  is the force acting on it in the direction of  $\beta$ , and  $r_{i\alpha}$  is its coordinate in the  $\alpha$  axis;  $\alpha$  and  $\beta$  denote  $x$ ,  $y$ , or  $z$  in a Cartesian reference

system. The pressure tensor elements were saved every 2 fs during the *NVT* simulation. Instead of determining the viscosity from the integral directly, we fitted the time integration to a double-exponential function as previously suggested:<sup>9</sup>

$$\eta(t) = A\alpha\tau_1(1-e^{-t/\tau_1}) + A(1-\alpha)\tau_2(1-e^{-t/\tau_2})$$

where  $A$ ,  $\alpha$ ,  $\tau_1$ , and  $\tau_2$  are fitted parameters. This approach was asserted to help prevent the arbitrariness traditional data analysis schemes could induce and thus provide a more reliable estimate of solvent viscosity.

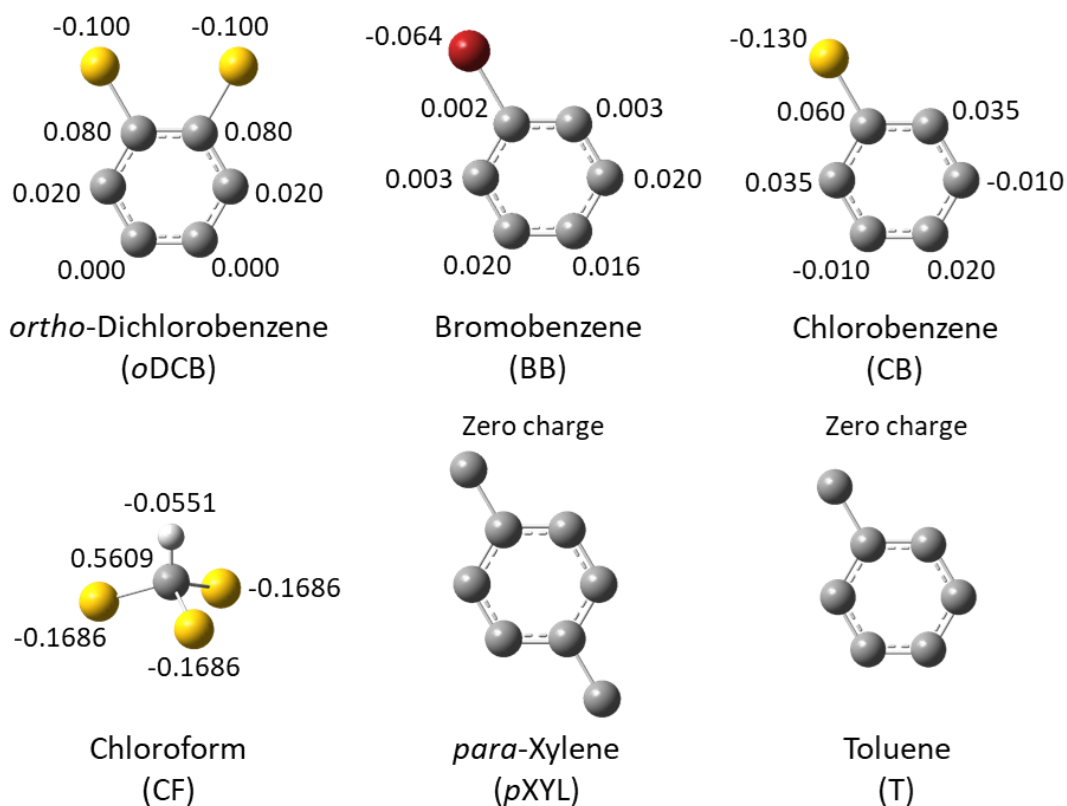


Fig. S1 Chemical structures of *ortho*-dichlorobenzene (oDCB), bromobenzene (BB), chlorobenzene

(CB), chloroform (CF), *para*-xylene (*p*XYL) and toluene (T), along with the distributions of partial atomic charges in unit of elementary charge ( $e$ ) on each solvent molecule.

Table S1 Physical properties of solvent molecules computed using AMD simulation data at 300 K and 1 bar and comparison with experimental data

		$\rho$ (g/cm <sup>3</sup> )	Exp. <sup>10</sup>	$D$ (10 <sup>-10</sup> m <sup>2</sup> /s)	Exp. <sup>11,12</sup>	$\eta$ (cp)	Exp. <sup>10</sup>
<i>o</i> DCB	w/	1.308 $\pm$ 0.003	1.306	10.57 $\pm$ 0.02	-	1.133	1.324
	w/o	1.307 $\pm$ 0.003		11.11 $\pm$ 0.03		1.030	
BB	w/	1.535 $\pm$ 0.008	1.495	12.51 $\pm$ 0.07	12.98	1.022	1.074
	w/o	1.536 $\pm$ 0.008		12.87 $\pm$ 0.07		1.065	
CB	w/	1.111 $\pm$ 0.003	1.106	18.45 $\pm$ 0.04	-	0.738	0.753
	w/o	1.109 $\pm$ 0.003		19.46 $\pm$ 0.05		0.645	
CF	w/	1.491 $\pm$ 0.006	1.479	25.72 $\pm$ 0.10	28.85	0.480	0.537
	w/o	1.477 $\pm$ 0.006		28.50 $\pm$ 0.08		0.402	
<i>p</i> XYL	w/o	0.863 $\pm$ 0.002	0.857	28.19 $\pm$ 0.08	-	0.518	0.603
T	w/o	0.867 $\pm$ 0.004	0.862	26.30 $\pm$ 0.06	25.45	0.566	0.560

### Poly(3-hexylthiophene) (P3HT)

The force field and parameter values describing the atomic interactions of a regioregular P3HT were taken from the simulation model developed by Bhatta *et al.*<sup>13</sup> This model adopted OPLS force field with torsional parameters and partial atomic charges computed from *ab initio* calculations. The computed crystalline structures, mass density, and melting point were all in good agreement with experimental measurements. As a further evaluation, the crystalline structure of P3HT was simulated under ambient

conditions (300 K and 1 bar), and a packing structure of non-interdigitated hexyl side chains was found (Fig. S2). The lattice parameters of  $a = 3.9 \text{ \AA}$ ,  $b = 3.8 \text{ \AA}$  and  $c = 16.9 \text{ \AA}$  were in excellent agreement with early experimental characterization,<sup>14</sup> where  $a$ ,  $b$ , and  $c$  denote the directions of P3HT backbone,  $\pi$ - $\pi$  stacking, and the hexyl side chain, respectively.

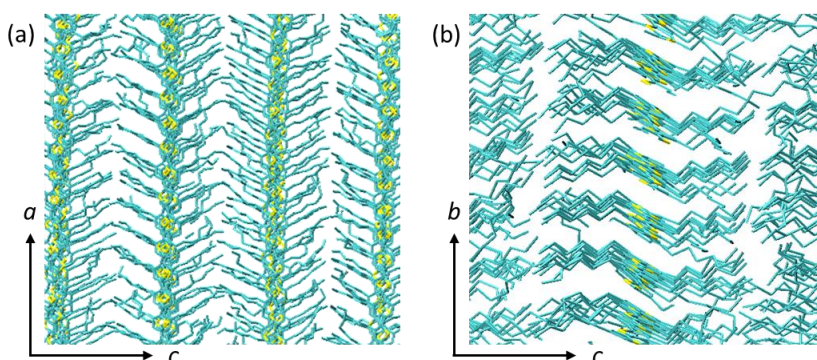


Fig. S2 Snapshots of the packing structure of 28 P3HT (30-mer, for comparison with an early theoretical characterization)<sup>15</sup> chains from AMD simulations performed at 300 K and 1 bar after 5 ns of the simulation: (a) top view with a  $\pi$ - $\pi$  stacking axis toward the viewer, and (b) top view with P3HT backbone axis toward the viewer. Hydrogen atoms are omitted for clarity.

## S2 Calculation of solvation free energy for P3HT dimers

Solvation Gibbs free energy ( $\Delta G$ ) is the free energy change associated with transferring a solute molecule from an ideal gas phase to the solution phase at a given temperature, pressure and solute concentration.

It describes the change of state between full and non-existent solute-solvent interactions and can be

evaluated by schemes such as thermodynamic integration (TI)<sup>16,17</sup> and free energy perturbation (FEP).<sup>18-</sup>

<sup>20</sup> The FEP method, first developed by Robert Zwanzig in 1954 for statistical mechanics of condensed phases,<sup>21</sup> comprises a variety of techniques that all rely on the sampling of overlapping configurational space. Among them, the exponential averaging (EXP) method

$$\Delta G_{ij} = -k_B T \ln \langle \exp(-[H(\lambda_j) - H(\lambda_i)]/k_B T) \rangle_{\lambda_i}$$

evaluates the difference of Hamiltonian,  $H$ , from  $\lambda$  states  $i$  and  $j$ , where  $\langle \dots \rangle_{\lambda_i}$  denotes the ensemble average over configurations sampled from the  $\lambda_i$  state. The sum of all partial results,  $\Delta G_{ij}$ , along the pathway of  $\lambda$  states from  $\lambda = 0$  to  $\lambda = 1$  yields the total free energy difference,  $\Delta G$ . However, the estimate of  $\Delta G_{ij}$  depends on whether  $\lambda_i$  or  $\lambda_j$  state is chosen as the reference. Alternatively, Bennett acceptance ratio (BAR) considers both perturbations sampled from  $\lambda_i$  and  $\lambda_j$  states in calculating  $\Delta G_{ij}$  in order to remove the bias in EXP<sup>18,19,22</sup> and was adopted in this study. The mean free energy and standard deviation were evaluated using ensemble averages from production data of  $N_b = 5$  blocks. The standard deviation,  $\sigma_{[\Delta G]}$ , was obtained by the following expression:<sup>18</sup>

$$\sigma_{[\Delta G]} = \sqrt{\frac{\sum_{i=1}^{N_b} (\Delta G_i - \Delta G)^2}{N_b(N_b - 1)}}$$

where  $\Delta G_i$  denotes the average free energy for the  $i$ th block.

In solvation free energy calculations, intermediate states are characterized by scaled solute-solvent interactions. Using the linear scaling, the Hamiltonian of an intermediate state is defined by

$$H(\lambda) = (1-\lambda)H_0 + \lambda H_1$$

with  $H_0$  and  $H_1$  being the Hamiltonian of full ( $\lambda = 0$ ) and no ( $\lambda = 1$ ) solute-solvent interactions. When inserting/removing a molecule in a dense solvent system, the effect of end-point singularity would lead to some numerical problems. In AMD simulations, repulsive interactions at small distances between the inserted/removed solute and the ambient solvent could hinder the sampling of the corresponding configurational space. Therefore, the interactions were interpolated via soft-core potentials (SCP) to flatten the curvature of  $H(\lambda)$ , while the electrostatic interactions were linearly interpolated between neighboring states during the decoupling process.<sup>16-18,23</sup> The SCP,  $V_{\text{SC}}(r)$ , is defined by

$$V_{\text{SC}}(r) = (1-\lambda)V_0(r_0) + \lambda V_1(r_1)$$

$$r_0 = (\alpha\sigma_0^6\lambda^p + r^6)^{1/6}$$

$$r_1 = (\alpha\sigma_1^6(1-\lambda)^p + r^6)^{1/6}$$

where  $V_0$  and  $V_1$  are the Lennard-Jones (LJ) potentials between two atoms at a distance of  $r$  for the fully coupled ( $\lambda = 0$ ) and decoupled ( $\lambda = 1$ ) states, respectively, and  $\alpha$  is the soft-core parameter which controls the softness of the interaction potential. It has been reported that 0.5 represents an optimum value for  $\alpha$  when the exponent  $p$  is unity.<sup>23,24</sup> These values, as employed in previous simulations,<sup>17,23,25,26</sup> were adopted in this study. We have also used 0.3 nm for the soft-core diameters of  $\sigma_0$  and  $\sigma_1$ , as previously suggested.<sup>23,26,27</sup>

For each solvent system, we first equilibrated a P3HT dimer with 500 solvent molecules (except for water, where 1000 molecules and TIP3P model were used) for a duration of 1 ns using *NPT* ensemble at 300 K and 1 bar, followed by the *NPT* production run for 3 ns. This procedure was repeated for several discrete  $\lambda$  values from  $\lambda = 0$  to  $\lambda = 1$ . Effects of finite box size were evaluated by also calculating the solvation free energy with 800 solvent molecules, confirming that the use of a smaller system with 500 solvent molecules is sufficient.<sup>18,28</sup> It has also been verified that the production run of 3 ns suffices to effectively sample all possible configurations, as a 5 ns test run produces similar results on solvation free energy. Because free energy is a state function, it is independent of the path taken for the transformation from the initial to final state. In practice, however, the choices of  $\lambda$  schedule could affect the precision of the computed free energy difference. First, the electrostatic interactions were decoupled before the van der Waals interactions were gradually turned off. This can help prevent two atoms of opposite charges from approaching closely enough to fall into the attractive singularity in the electrostatic potential.<sup>16,19,20,23</sup> The linear 5-window schedule ( $\lambda_{\text{elec}} = 0.00, 0.25, 0.50, 0.75, 1.00$ )<sup>20,28</sup> was used for electrostatic interactions, and the results are fairly identical to those using the 11-window schedule ( $\lambda_{\text{elec}} = 0.0, 0.1, 0.2, 0.3, 0.4, 0.5, 0.6, 0.7, 0.8, 0.9, 1.0$ ).<sup>17,23</sup> For van der Waals interactions, 16-window schedule ( $\lambda_{\text{vdW}} = 0.00, 0.05, 0.10, 0.20, 0.30, 0.40, 0.50, 0.60, 0.65, 0.70, 0.75, 0.80, 0.85, 0.90, 0.95, 1.00$ ) was used, as suggested in prior work.<sup>28</sup> As there existed no reported values for the solvation free energy of P3HT dimer, we have also computed the hydration free energy of methane as well as the

solvation free energy of toluene in the CF medium. The results,  $9.3 \pm 0.2$  and  $-22.9 \pm 0.1$  kJ/mole, respectively, are in excellent agreement with previously reported values ( $9.2 \pm 0.6$  and  $-25.1 \pm 1.3$  kJ/mole, respectively).<sup>27</sup>

To gain further insight into the solvation process of P3HT, the solvation free energy was decomposed into entropic and enthalpic contributions. The change of entropy at a temperature  $T$  can be computed using the standard relationship

$$\Delta S(T) = -\left(\frac{\partial \Delta G}{\partial T}\right)_{P,N}$$

Using finite-difference (FD) schemes,<sup>29,30</sup> the above relationship can be approximated by

$$\Delta S(T) = -\frac{\Delta G(T+\Delta T) - \Delta G(T-\Delta T)}{2\Delta T}$$

Thus, we have performed independent simulations at each of the three temperatures  $T-\Delta T$ ,  $T$  and  $T+\Delta T$ , where  $\Delta T$  is 50 K. This FD approximation is based on the assumption that heat capacity is nearly constant over a range of temperatures near  $T$ . For aqueous solutions, this assumption usually holds valid near the room temperature with  $\Delta T$  as large as 50 K.<sup>29,30</sup> The choice of  $\Delta T$  is important to minimize the statistical uncertainty associated with the FD approximation, with the statistical uncertainty for entropy being inversely proportional to  $\Delta T$  according to the following relationship:<sup>29</sup>

$$\sigma_{[T\Delta S(T)]} = \frac{T}{2\Delta T}(\sigma_{[\Delta G(T+\Delta T)]} + \sigma_{[\Delta G(T-\Delta T)]})$$

where  $\sigma_{[\Delta G(T)]}$  is the standard deviation associated with the Gibbs free energy of solvation at the temperature  $T$ . Thus, as  $\Delta T$  becomes smaller, more expensive computations will be required to achieve

convergent results on the entropy of solvation. When  $\Delta T$  is too large, on the other hand, the accuracy of the FD approximation deteriorates due to the failure of the linearity assumption of the free energy changes over the range of temperatures under consideration. The change of enthalpy,  $\Delta H(T)$ , is obtained using the difference between  $\Delta G(T)$  and  $-T\Delta S(T)$ , with the statistic error evaluated using the sum of the statistical uncertainties of the two quantities.

### S3 Static and dynamic properties of P3HT solutions with/without partial atomic charges

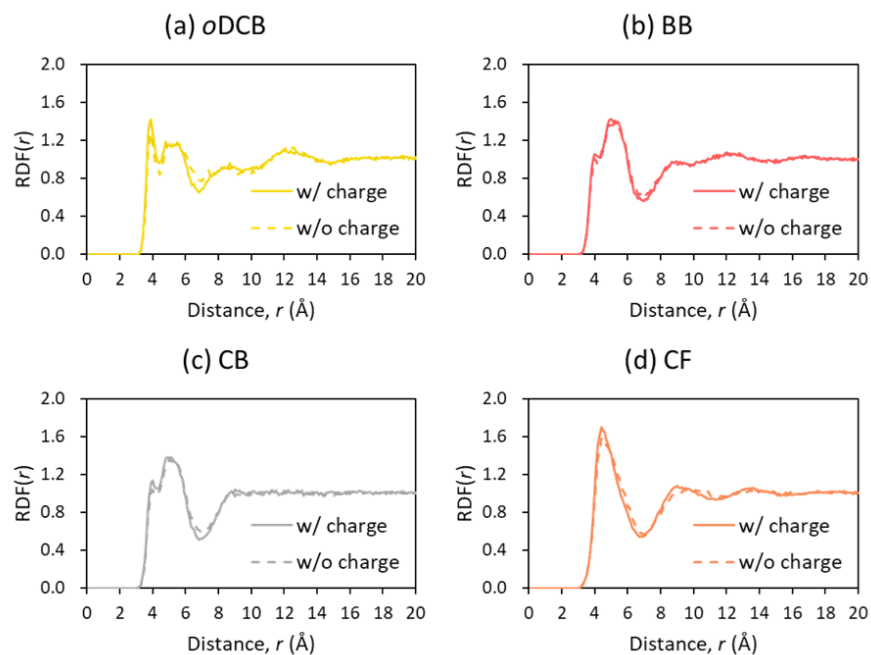


Fig. S3 Radial distribution functions for (a) P3HT-*o*DCB, (b) P3HT-BB, (c) P3HT-CB and (d) P3HT-CF pairs with (solid lines) or without (dashed lines) including partial atomic charges for both polymer and solvent species.

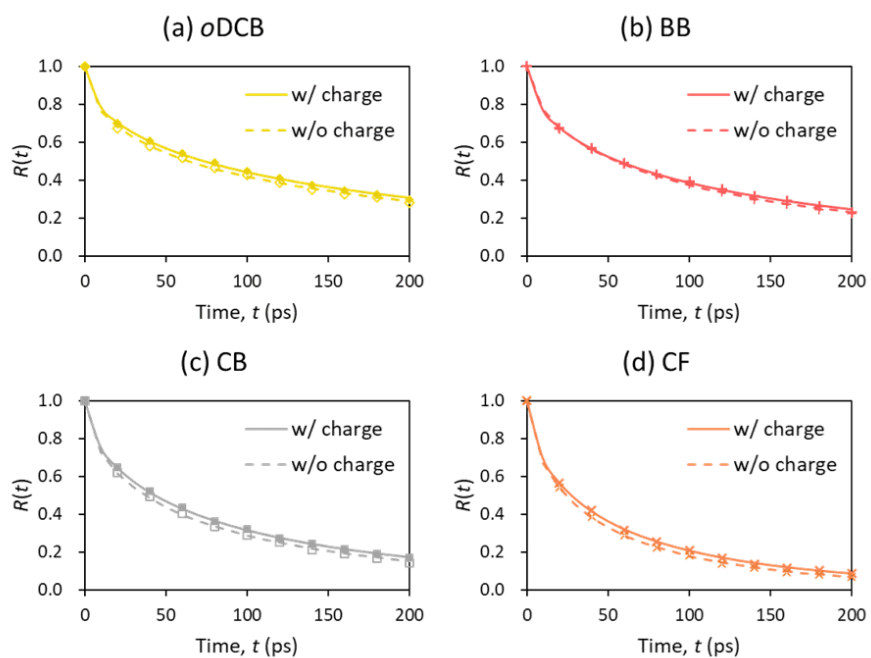


Fig. S4 Occupation time correlation functions for (a) *o*DCB, (b) BB, (c) CB and (d) CF molecules residing in the first solvation shells with (solid lines) or without (dashed lines) including partial atomic charges for both polymer and solvent species.

#### S4 Evaluation of various diffusivities of single P3HT chains

The mass-center diffusivity ( $D$ ) of single P3HT chains may be evaluated through the time-dependent mean-square displacements (MSDs):

$$\text{MSD} = \langle |r(t) - r(0)|^2 \rangle = 6Dt$$

where  $r(t)$  and  $r(0)$  denote the positions of the mass center of a P3HT chain at times  $t$  and 0, respectively.

Simulation data were gathered when the MSDs notably exceed the square of the mean radius of gyration of the P3HT chain ( $\sim 1.72$  nm in all solvent media). Fig. S5 shows the simulation data of  $\text{MSD}/t$  vs.  $t$  for all six solvent media, and the chain diffusivity in each case is estimated when  $\text{MSD}/t$  reaches a plateau at times 8 ~ 10 ns. The diffusivities so obtained are gathered in Table S2.

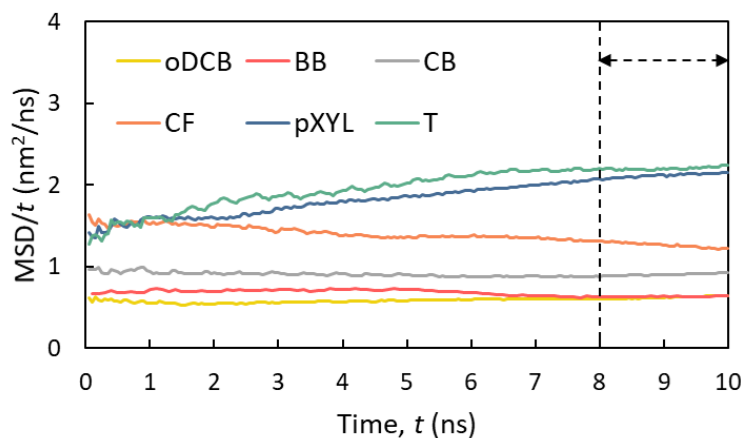


Fig. S5 Time-dependent  $\text{MSD}/t$  of single P3HT chains in *o*DCB (yellow), BB (red), CB (gray), CF (orange), *p*XYL (blue) and T (green) media; the double-head arrows indicate the time domain used to estimate chain diffusivities.

Because of relatively short and, hence, rigid P3HT chains investigated herein, the translational diffusion is further decomposed into ones that are parallel ( $D_{\parallel}$ ) and perpendicular ( $D_{\perp}$ ) to the polymer backbone axis, respectively. The anisotropic translational diffusivities were evaluated using schemes

described in an early study on liquid benzenes.<sup>31</sup> The unit end-to-end vector of the P3HT chain was used to define the motion parallel to the polymer backbone axis. Another vector that is orthogonal to a plane formed by this vector and the thiophene normal (which represents the average normal direction of all thiophenes on a chain) was used to define the motion perpendicular to the polymer backbone axis. The respective displacements were then obtained by decomposition of the overall mass-center displacement along the two directions. The displacements so obtained were discretized for every 50 ps, and the results were summed up and averaged to yield  $MSD_{\parallel}$  and  $MSD_{\perp}$  as a function of time. The  $D_{\parallel}$  and  $D_{\perp}$  can then be evaluated by the formula

$$MSD_i = \langle |r_i(t) - r_i(0)|^2 \rangle = 2D_i t$$

where  $i$  denotes the parallel or perpendicular component. Statistical data collected during the interval 8 ~ 10 ns were used to estimate the anisotropic diffusivities of a P3HT chain; see Table S2.

Note that the anisotropic diffusivities obtained using the methods described above should be considered as “effective” ones, as they were computed as if the polymer chain was restrained from reorienting.<sup>31</sup> Thus, the results should not be directly compared with the mass-center diffusivity.

Table S2 Parallel ( $D_{\parallel}$ ) and perpendicular ( $D_{\perp}$ ) translational diffusivities and mass-center diffusivity ( $D$ ) of a P3HT chain at 300 K and 1 bar in various solvent media

( $10^{-10} \text{ m}^2/\text{s}$ )	$D_{\parallel}$	$D_{\perp}$	$D$
<i>o</i> DCB	$2.20 \pm 0.08$	$1.28 \pm 0.04$	$1.04 \pm 0.01$
BB	$1.03 \pm 0.04$	$0.99 \pm 0.02$	$1.06 \pm 0.03$
CB	$1.62 \pm 0.10$	$1.30 \pm 0.04$	$1.51 \pm 0.02$
CF	$2.69 \pm 0.06$	$2.20 \pm 0.07$	$2.10 \pm 0.03$
<i>p</i> XYL	$2.99 \pm 0.04$	$2.16 \pm 0.06$	$3.53 \pm 0.03$
T	$4.71 \pm 0.13$	$2.59 \pm 0.07$	$3.67 \pm 0.05$

**S5 Correlations of calculated solvent viscosity with solvation shell relaxation time and chain mobility, respectively**

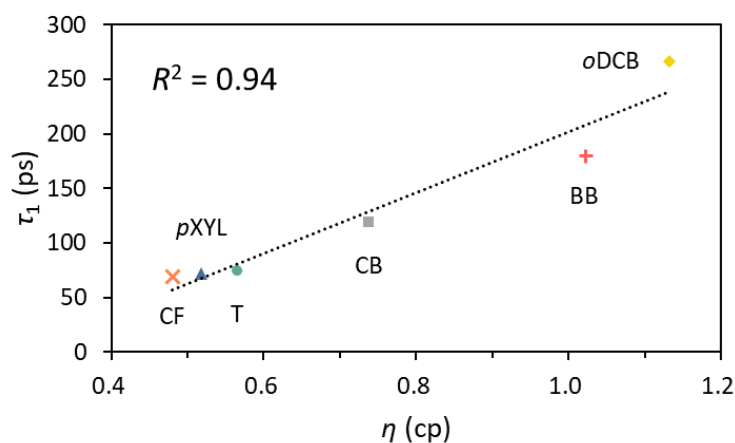


Fig. S6 Correlation between the calculated solvent viscosity and the mean relaxation time of the first solvation shell for *o*DCB, BB, CB, CF, *p*XYL and T as the solvent medium. An approximately linear relationship between the two can be seen.

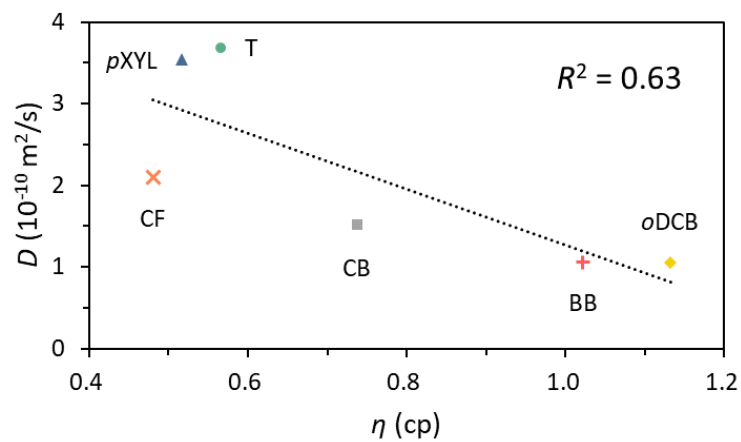


Fig. S7 Correlation between the calculated solvent viscosity and the mass-center diffusivity of P3HT chain for *o*DCB, BB, CB, CF, *p*XYL and T as the solvent medium. The linear relationship predicted by the Stokes-Einstein relation clearly does not apply for the P3HT solutions investigated.

## References

- 1 C. I. Wang and C. C. Hua, *J. Phys. Chem. B*, 2015, **119**, 14496-14504.
- 2 W. L. Jorgensen, D. S. Maxwell and J. Tirado-Rives, *J. Am. Chem. Soc.*, 1996, **118**, 11225-11236.
- 3 T. M. Chang, L. X. Dang and K. A. Peterson, *J. Phys. Chem. B*, 1997, **101**, 3413-3419.
- 4 G. Kamath, G. Georgiev and J. J. Potoff, *J. Phys. Chem. B*, 2005, **109**, 19463-19473.
- 5 N. Rai and J. I. Siepmann, *J. Phys. Chem. B*, 2013, **117**, 273-288.
- 6 C. D. Wick, M. G. Martin and J. I. Siepmann, *J. Phys. Chem. B*, 2000, **104**, 8008-8016.
- 7 D. Nevins and F. J. Spera, *Mol. Simul.*, 2007, **33**, 1261-1266.
- 8 G. S. Fanourgakis, J. S. Medina and R. Prosimiti, *J. Phys. Chem. A*, 2012, **116**, 2564-2570.
- 9 Y. Zhang, A. Otani and E. J. Maginn, *J. Chem. Theory Comput.*, 2015, **11**, 3537-3546.
- 10 D. R. Lide, *CRC Handbook of Chemistry and Physics*, CRC Press/Taylor and Francis, Boca Raton, Florida, 90 edn., 2009.
- 11 H. Ertl and F. A. L. Dullien, *AIChE J.*, 1973, **19**, 1215-1223.
- 12 S. A. Sanni and P. Hutchison, *J. Chem. Eng. Data*, 1973, **18**, 317-322.
- 13 R. S. Bhatta, Y. Y. Yimer, D. S. Perry and M. Tsige, *J. Phys. Chem. B*, 2013, **117**, 10035-10045.
- 14 T. J. Prosa, M. J. Winokur, J. Moulton, P. Smith and A. J. Heeger, *Macromolecules*, 1992, **25**, 4364-4372.
- 15 O. Alexiadis and V. G. Mavrantzas, *Macromolecules*, 2013, **46**, 2450-2467.
- 16 M. R. Shirts, J. W. Pitera, W. C. Swope and V. S. Pande, *J. Chem. Phys.*, 2003, **119**, 5740-5761.
- 17 N. M. Garrido, A. J. Queimada, M. Jorge, I. G. Economou and E. A. Macedo, *Fluid Phase Equilib.*, 2010, **296**, 110-115.
- 18 A. Mecklenfeld and G. Raabe, *Mol. Phys.*, 2017, **115**, 1322-1334.
- 19 P. V. Klimovich, M. R. Shirts and D. L. Mobley, *J. Comput. Aided Mol. Des.*, 2015, **29**, 397-411.
- 20 D. Shivakumar, J. Williams, Y. Wu, W. Damm, J. Shelley and W. Sherman, *J. Chem. Theory Comput.*, 2010, **6**, 1509-1519.
- 21 R. W. Zwanzig, *J. Chem. Phys.*, 1954, **22**, 1420-1426.
- 22 A. Pohorille, C. Jarzynski and C. Chipot, *J. Phys. Chem. B*, 2010, **114**, 10235-10253.
- 23 L. Yang, A. Ahmed and S. I. Sandler, *J. Comput. Chem.*, 2013, **34**, 284-293.
- 24 T. Steinbrecher, I. Joung and D. A. Case, *J. Comput. Chem.*, 2011, **32**, 3253-3263.
- 25 T. Steinbrecher, D. L. Mobley and D. A. Case, *J. Chem. Phys.*, 2007, **127**, 214108.
- 26 M. Lundborg and E. Lindahl, *J. Phys. Chem. B*, 2015, **119**, 810-823.
- 27 A. Villa and A. E. Mark, *J. Comput. Chem.*, 2002, **23**, 548-553.
- 28 S. Parameswaran and D. L. Mobley, *J. Comput. Aided Mol. Des.*, 2014, **28**, 825-829.
- 29 M. M. Kubo, E. Gallicchio and R. M. Levy, *J. Phys. Chem. B*, 1997, **101**, 10527-10534.
- 30 S. Wan, R. H. Stote and M. Karplus, *J. Chem. Phys.*, 2004, **121**, 9539-9548.

31 M. Schwartz, D. Duan and R. J. Berry, *J. Phys. Chem. A*, 2005, **109**, 8637-8641.